Radiation Physics and Chemistry 137 (2017) 144–150

Contents lists available at ScienceDirect

Radiation Physics and Chemistry

journal homepage: www.elsevier.com/locate/radphyschem

A comparison of two prompt gamma imaging techniques with collimator-based cameras for range verification in proton therapy

Hsin-Hon Lin [a,b,1], Hao-Ting Chang [a,1], Tsi-Chian Chao [c], Keh-Shih Chuang [a,*]

[a] Department of Biomedical Engineering & Environmental Sciences, National Tsing-Hua University, 101, Sec. 2, Kuang-Fu Rd., Hsinchu 30013, Taiwan
[b] Medical Physics Research Center, Institute for Radiological Research, Chang Gung University/Chang Gung Memorial Hospital, Taoyuan, Taiwan
[c] Department of Medical Imaging and Radiological Sciences, College of Medicine, Chang Gung University, Taoyuan, Taiwan

HIGHLIGHTS

- Collimator-based cameras for range verification in proton therapy are compared.
- The knife-edge system achieves higher efficiency and lower influence of neutron contamination.
- The multi-slit system has sharper slope in distant falloff of PG distribution.
- Both collimator systems achieve reasonable accuracy in range prediction.

ARTICLE INFO

Article history:
Received 29 November 2015
Received in revised form
10 April 2016
Accepted 29 April 2016
Available online 29 April 2016

Keywords:
Proton therapy
Range verification
Prompt gamma
Collimator-based camera

ABSTRACT

In vivo range verification plays an important role in proton therapy to fully utilize the benefits of the Bragg peak (BP) for delivering high radiation dose to tumor, while sparing the normal tissue. For accurately locating the position of BP, camera equipped with collimators (multi-slit and knife-edge collimator) to image prompt gamma (PG) emitted along the proton tracks in the patient have been proposed for range verification. The aim of the work is to compare the performance of multi-slit collimator and knife-edge collimator for non-invasive proton beam range verification. PG imaging was simulated by a validated GATE/GEANT4 Monte Carlo code to model the spot-scanning proton therapy and cylindrical PMMA phantom in detail. For each spot, 10^8 protons were simulated. To investigate the correlation between the acquired PG profile and the proton range, the falloff regions of PG profiles were fitted with a 3-line-segment curve function as the range estimate. Factors including the energy window setting, proton energy, phantom size, and phantom shift that may influence the accuracy of detecting range were studied. Results indicated that both collimator systems achieve reasonable accuracy and good response to the phantom shift. The accuracy of range predicted by multi-slit collimator system is less affected by the proton energy, while knife-edge collimator system can achieve higher detection efficiency that lead to a smaller deviation in predicting range. We conclude that both collimator systems have potentials for accurately range monitoring in proton therapy. It is noted that neutron contamination has a marked impact on range prediction of the two systems, especially in multi-slit system. Therefore, a neutron reduction technique for improving the accuracy of range verification of proton therapy is needed.

1. Introduction

Proton therapy uses high energy proton beam for cancer treatment and is known for its theoretically superior radiation dose benefits compared to photons due to the low entrance dose and the sharp Bragg peak (BP) at the end of the proton range (Lomax et al., 2004). However, range uncertainties in the proton beam may lead to target underdose or normal tissue overdose (Smith, 2009). As a result, additional margins are required to ensure adequate target coverage, thus reducing the superiority of protons over photons. In order to fully utilize the potential advantage of proton therapy, the range of proton beams in the patient needs to be predicted as accurately as possible in the delivering process. The range verification with in-vivo measurements would provide additional information about the treatment and could lead to a reduction of margins (Paganetti, 2012).

Prompt gamma (PG) is emitted in the decay process from an excited nucleus to its ground state following proton–nuclear

* Corresponding author.
E-mail address: kschuang@mx.nthu.edu.tw (K.-S. Chuang).
[1] H.H. Lin and H.T. Chang contributed equally to this work.

http://dx.doi.org/10.1016/j.radphyschem.2016.04.020
0969-806X/

interaction. There is a strong correlation between the region of PG emission and dose deposition by the proton beam. Therefore, detection of the PG enabled the accurate determination of the proton range (Min et al., 2012). This is a promising method for *in vivo* range verification of proton (Min et al., 2006). PG measurements including Compton camera system (active shielding) (Peterson et al., 2010) and collimator-based camera (passive shielding) (Gueth et al., 2013; Smeets et al., 2012) have been performed over the last few years. The former uses multistage detectors for cascade photon detection and can provide three-dimensional prompt gamma image. However, due to the inefficiency in detecting the high energy PG, the Compton camera is very low in sensitivity and less effective in range verification with clinically acceptable dose rates at present. The latter shows a relatively simple design for range verification in proton therapy. Although, current collimator-based cameras merely provide one-dimensional imaging and prone to neutron contamination, the higher efficiency and more accurately retrieved information about the proton range have been verified as a quite feasible method in clinical application by several research groups (Gueth et al., 2013; Smeets et al., 2012).

In this study, we focused on prompt gamma imaging with collimator-based cameras including multi-slit collimator (Gueth et al., 2013) and knife-edge collimator (Smeets et al., 2012) for range verification. Although both PG detection systems are being studied by several groups, work comparing these two systems is limited (Cambraia Lopes et al., 2012). To this end, our goal is to evaluate the performance of the two PG detection systems as an independent tool for non-invasive proton beam range verification. This paper is organized as follows. Section 2.1 gives details on the simulation parameters used for the used Monte Carlo codes. Sections 2.2, 2.3 describe, respectively, the common set-up, and the procedure of data analysis in detection profile. Results are given in Section 3 that evaluate the dependence of the performance of the two PG cameras on different parameters including proton energy, phantom sizes, and phantom shifts. Advantages and limitations are discussed in Section 4.

2. Materials and methods

2.1. Monte-Carlo simulations

The GATE platform, based on GEANT4 toolkit, is an MC simulation application enabling modeling of emission tomography, transmission tomography and extending to radiation therapy recently (Jan et al., 2011). The GATE platform can provide both features of radiotherapy application and modeling of complex collimator/detector, making it easy to meet our anticipated needs for studying prompt gamma imaging during proton therapy within the same framework. GATE version 6.1, based on GEANT4 version 9.4 p01, was used. We used the physics list proposed by (Grevillot et al., 2011), which considered both electromagnetic process and hadronic process. For electromagnetic process, the Opt3 electromagnetic standard package parameters were selected. G4UHadronElasticProcess combined with the G4HadronElastic model was used for elastic hadronic (HAD) interactions and Binary Cascade (BC) model for inelastic HAD interactions. The BC model was used for energies higher than 14 MeV, and high precision neutron package (Neutron HP) was used to transport neutrons down to thermal energies for neutrons. The range cut-off for gamma, electrons and positrons was set to be 0.1 mm.

Although this work focuses on the comparison of collimator-based PG systems under the same MC simulation environment, the hadronic models used by this study needed to be benchmarked. Such validation was performed by comparing GATE simulations with the yields and energy distributions of secondary particles reported by (Robert et al., 2013). We reproduced the experimental set up used by Robert et al., which is performed by using a perfect line beam of 10^7 protons irradiating a PMMA phantom ($C_5H_8O_2$, $10 \times 10 \times 60$ cm^3). The comparison of yields of secondary particles exiting from the target obtained by Robert et al. and the current model was listed in Table 1. The current MC model underestimated the yields of secondary particles (up to ~8%) as obtained by Robert et al., but the photon-to-neutron ratio between the two is found quite close. The shapes of the energy distributions are similar to those of Robert et al., (Fig. 1); All the major gamma lines are reliably reproduced by our MC model, despite the slight discrepancies in the magnitude of each gamma line.

Table 1
Comparison of yields of outgoing particles per primary particle obtained by Robert et al. and the current model for a 134 MeV proton beam irradiating a homogeneous PMMA phantom.

Particles	Current model	Robert et al.
Photon (> 1 MeV)	0.086895	0.094496
Neutron	0.082304	0.087136
Proton	0.001200	0.001292

2.2. Simulation setup for the prompt gamma imaging

Fig. 2 illustrates the configurations for the multi-slit system (Gueth et al., 2013) and the knife-edge system (Smeets et al., 2012). For both systems, the volume of detector was $360 \times 400 \times 50$ mm^3 (transaxial, axial and depth directions) with each LYSO crystal of size $2 \times 2 \times 50$ mm^3. The detector was located at 600 mm from the phantom perpendicular to the beam direction. Both collimators were placed halfway between the phantom and detector to create a 1:1 projected image of the PG. The collimator in the multi-slit system consisted of 100 lead septa each with size of $2 \times 400 \times 200$ mm^3 (Min et al., 2012) and space of 2 mm. The knife-edge collimator was similar to a slit collimator with thickness of 60 mm, height 400 mm, and a total volume of $400 \times 400 \times 60$ mm^3. The slit width was 6 mm with slit angle of 63° (Smeets et al., 2012).

We simulated a mono-energetic Gaussian proton pencil beam (FWHM = 11.775 mm) directly incident onto the center of a 200 mm long cylindrical PMMA phantom. A single spot of 10^8 protons was considered for each simulation run. Five realizations

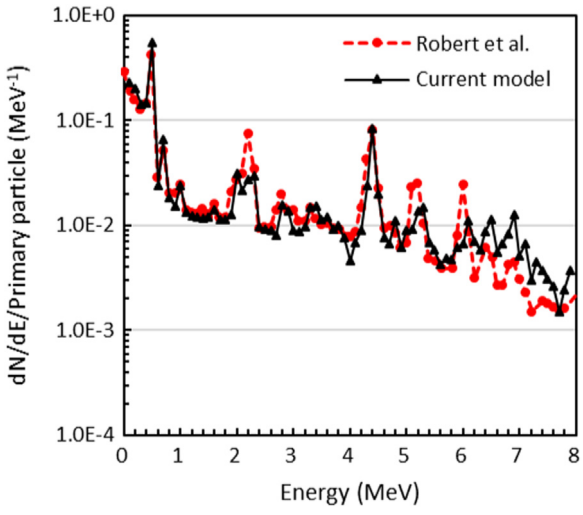

Fig. 1. Outgoing photon energy distributions per primary particle exiting from the PMMA target obtained by the current model and Robert et al.

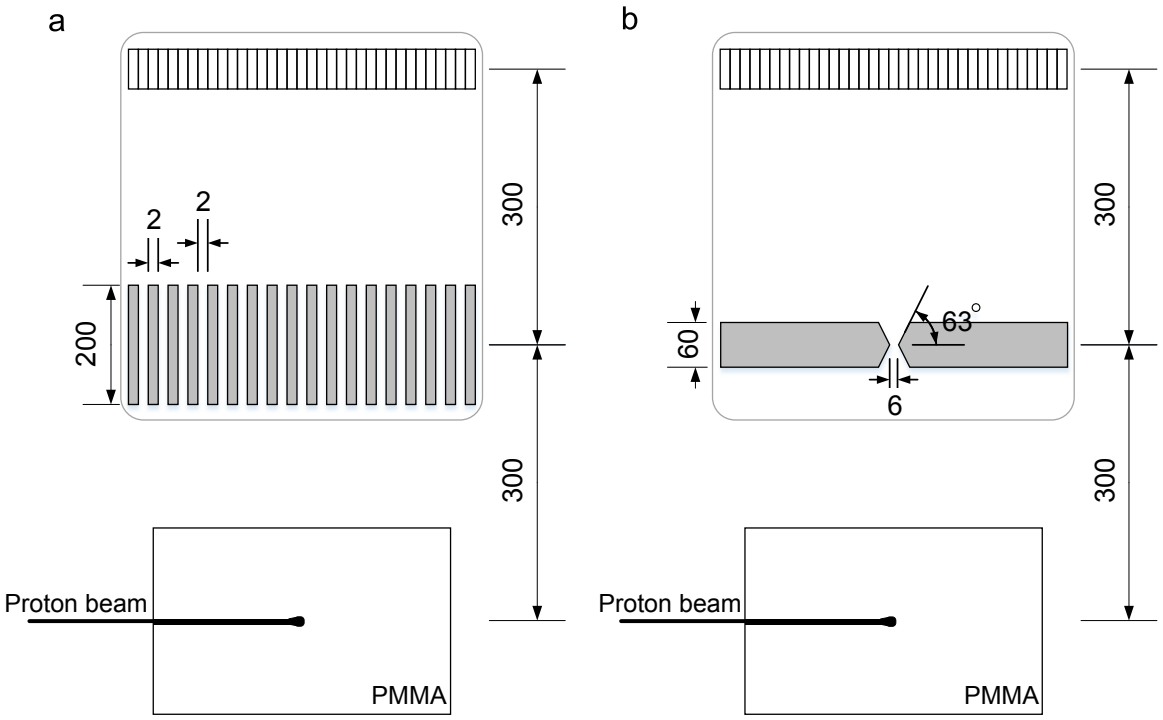

Fig. 2. The system configurations for (a) multi-slit and (b) knife-edge collimator-based cameras. Both collimators were located halfway between the phantom and detector. All units were measured in mm.

were carried out for the simulation of each configuration.

2.3. Detection profiles and data analysis

Min et al. were the first to verify the correlation between detection profile and proton range using a collimator-based system at 90° with respect to the proton beam (Min et al., 2006). In this study, the PG distribution was detected at 90° through the lateral collimator with a 2 mm resolution for both systems. The detection profile represented the proton depth-dose along the direction of proton beam. The Bragg peak (proton range) was defined as 50% of the distal dose falloff (Gueth et al., 2013) and was determined from the detection profile.

As depicted in Fig. 3, four characteristic points (x_i, y_i) were identified from the profile based on the slope change. Then, the detection profile was approximated by the 3-line-segment curve using the four characteristic points (Smeets et al., 2012). From these characteristic points, we could derive peak, delta, baseline and range as (y_2-y_3), (x_3-x_2), $(y_3+y_4)/2$, $(x_2+x_3)/2$, respectively. The baseline was related to the background signals, mainly caused by the prompt gammas penetrating the collimator, neutrons passing through the collimator and particles that are scattered or interact with the collimator producing secondaries. The higher the ratio between the peak and delta, the more accurate would be the determination of proton range (50% distal falloff). To achieve a better outcome of proton therapy, both a low background sensitivity and a highly accurate prediction of proton range were desirable.

3. Results

In the first part, we analyzed the characteristics of the detection profiles and optimized the energy window based on identical geometric configurations for both PG detection systems. The performances of the two systems under different circumstances were then compared.

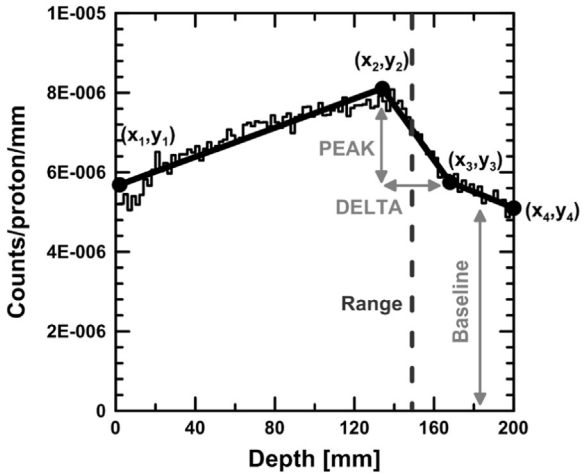

Fig. 3. The detection profile was fitted with a 3-line-segment curve by locating the four characteristic points (x_i, y_i). The peak, delta, baseline and range were derived from the fitting.

3.1. Detection profile and energy window setting

In this section, the PG imaging with multi-slit or knife-edge collimator systems were simulated using a 160 MeV proton beam incident on the PMMA phantom of 150 mm diameter. Fig. 4 compares the detection profiles (photon plus neutron) and its neutron component of both systems in different energy windows. Note that only the photon and neutron were scored in the detection profiles, since the relative contributions from other particles are small and neglected in the study.

All profiles showed a marked drop at the end, indicating a suitable proton distal falloff for range detection. The detected counts in the multi-slit system were much smaller and were about half of those in knife-edge system. As shown in Fig. 4(b), the knife-edge system had higher detection efficiency and a larger peak, while the multi-slit system had a smaller delta (sharper slope) and

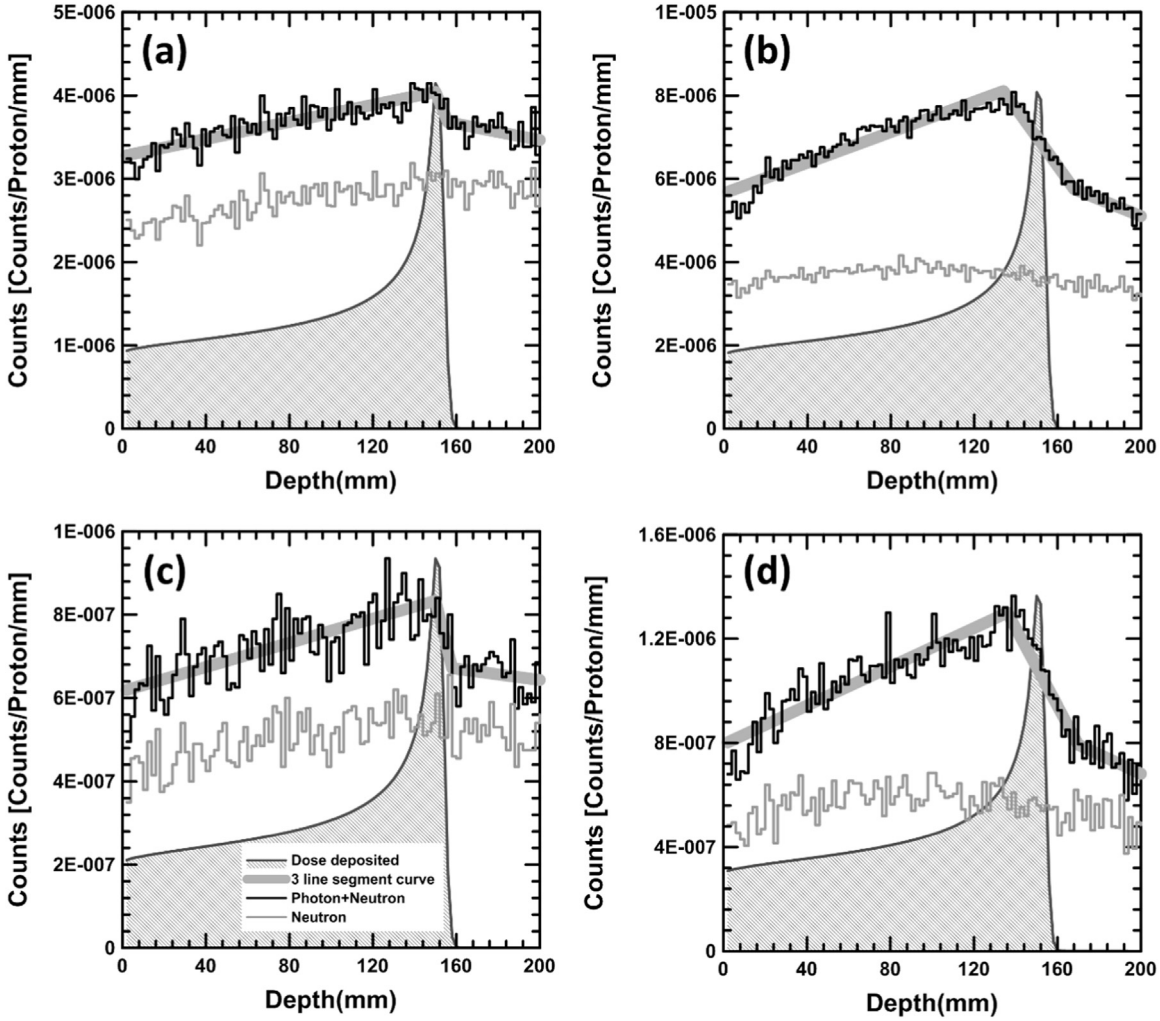

Fig. 4. Detection (photon + neutron) profile (dark line) and neutron profile (gray line) of a 160 MeV pencil beam with the multi-slit system (left) and the knife-edge system (right) are fitted with a 3-line-segment curve. The upper figures (top) are total counts with energies from 0 to 20 MeV while figures (c) is from 2 to 7 MeV PG and figure (d) is from 3 to 7 MeV PG.

a smaller baseline (Fig. 4(a)). It's worth pointing out that the multi-slit system has a higher neutron-to-photon ratio due to its lower photon detection efficiency compared to knife-edge system, although its neutron contamination is smaller than those of knife-edge system. This also indicate the degradation of PG images from neutron contamination is more noticeable in the case of the multi-slit system.

Note that the delta was larger in knife-edge system that may lead to less accurate range detection. However, thanks to its higher efficiency and peak, the knife-edge system still gives a smaller error in proton range detection (ΔRange (mean ± SD): multi-slit = 1.23 ± 0.85 mm and knife-edge = −0.77 ± 0.49 mm). Thus, the photon count (peak) plays an important role in assessing the performance of PG systems.

Fig. 4(a) and (b) shows that the neutron contamination is the main source of the background signal and had a great influence on the profile detection for collimator-based PG system. The significant amount of high energy spallation neutrons and the associated background gammas would affect the measurement. Therefore, the determination of the optimal energy window is required for each PG systems in order to enable selective measurement of the prompt gammas, effectively discriminating the unwanted neutron and background gammas. After optimization considering the slope in the distal falloff region, the energy window of 2–7 MeV for multi-slit system has highest correlation with the BP position, while 3–7 MeV for knife-edge system. As illustrated in Fig. 4(c)–(d), the delta was greatly reduced and the range was more accurately detected (ΔRange (mean ± SD): multi-slit = −0.47 ± 1.41 mm, knife-edge = −0.67 ± 1.6 mm) for both systems under the optimized energy window.

3.2. Proton energy

To investigate the effect of proton energy on PG detection in both systems, the proton pencil beam with three representative proton energies (50, 100, and 160 MeV) were simulated to irradiate the center of a cylindrical PMMA phantom of 150 mm diameter. The parameters derived from the detection profiles were tabulated in Table 2. In general terms, the baseline increase as proton energy increases, leading to the decrease of the peak; no significant change in delta were found for both systems. Compared to the multi-slit system, the range predicted by knife-edge system was susceptible to the change of proton energy, especially in low energy (50 MeV). The reason can probably be understood as follows: since knife-edge system has larger delta value, its range determination was more prone to large error for the low energy proton beam, which yielded a limited detection profiles.

Table 2
Parameters estimated by a 3-line-segment curve on the detection profiles of 50, 100, and 160 MeV proton beam for both systems.

Collimator	Energy (MeV)	Peak[a]	Delta (mm)	Baseline[a]	ΔRange (mm)
Multi-slit	50	1.62 ± 0.17	12.00 ± 1.41	0.28 ± 0.01	-0.62 ± 0.55
	100	1.33 ± 0.15	11.20 ± 3.63	2.46 ± 0.08	0.22 ± 1.82
	160	1.30 ± 0.29	6.40 ± 11.78	6.71 ± 0.10	-0.47 ± 1.58
Knife-edge	50	4.25 ± 0.10	32.80 ± 2.28	0.46 ± 0.02	5.38 ± 1.52
	100	5.81 ± 0.14	35.60 ± 0.89	2.58 ± 0.02	0.82 ± 1.41
	160	4.95 ± 0.09	35.60 ± 0.89	7.37 ± 0.01	-1.47 ± 1.41

[a] The unit of the Peak and Baseline is counts $\times 10^{-7}$/proton/mm.

3.3. Phantom size

Four different sizes of phantom (with diameter of 100, 150, 200, and 300 mm) with the irradiation of 160 MeV proton beam were simulated to study the range verification in both systems. Table 3 tabulates the estimated parameters and range deviation for various phantom sizes. It is shown that for the two systems, both peak and baseline decrease as phantom size increases due to the increasing attenuation of PG, while no obvious change in delta. No significant deviation in the detection of range for various sizes of phantom in both systems. These results indicate that both collimator systems can be applied to different object size without degrading the accuracy of range prediction.

3.4. Range shift

To evaluating the ability of the two PG systems detecting shifts of the proton beam range in the target, we shifted the phantom with different distance and measured the corresponding range shift of the detection profile in the scintillator. The simulated setup included a pencil beam of 160 MeV protons incident upon a cylindrical PMMA phantom with diameter of 150 mm. The phantom was shifted $0, \pm 1, \pm 2, \pm 3, \pm 4, \pm 5, \pm 10, \pm 15, \pm 20$ mm along the beam direction. The detected range shift is defined as the difference between the detected range and the reference range (which is the range without shifting). Fig. 5(a) plots the detected range shift versus the phantom shift. The result shows a positive association between the phantom shift and the detected range shift. However, there are deviations from a strict linear relationship. The deviations can be corrected by the use of a polynomial equation.

A second order polynomial ($\Delta R = B_2(\Delta x)^2 + B_1(\Delta x) + B_0$) was used to model the relationship between detected range shift (Δx) and the phantom shift (ΔR) (Smeets et al., 2012). This relationship can be established before actual treatment. From this polynomial, we obtained the corrected range shift ($\Delta R'$). Thus the difference between ΔR and $\Delta R'$ were computed over the phantom shifts studied (within ± 20 mm). The standard deviation (SD) of the modified shift was 3.82 and 2.46 mm for multi-slit and knife-edge, respectively. Fig. 5(b) shows a pretty linear relationship between phantom shift and the detected range shift in both systems after the shift correction and the standard deviation in knife-edge system was reduced significantly.

The neutron contamination is one of the major factors in range shift detection. In both collimator-based PG detection systems, a considerable background signal induced by neutrons obscures the prompt gamma image. Fig. 5(c) displays the results without neutron contamination and an excellent linear relationship between phantom shift and the detected profile shift was observed for the multi-slit system. However, a slight distortion of range prediction in the knife-edge system can be observed due to the location-dependent solid angle of knife-edge system together with the beam direction. After the shift correction process (Fig. 5(d)), both systems provided near perfect results when complete neutron rejection can be achieved (SD: multi-slit = 1.87 mm and knife-edge = 1.76 mm).

4. Discussion and conclusions

We compared the performance of both systems under various situations. This comparison is established on the basis of the same scintillator detector array to image the same field of view (FOV) with both cameras under an equivalent magnification factor. From the characteristics of detection profiles, it is shown that knife-edge system provides higher peak, baseline, smaller deviation in range determination, and less influence of neutron contamination. By contrast, the multi-slit system has smaller delta and its range determination is less energy dependent.

To minimize the background signals of collimator-based PG systems and improve the distal falloff slope, we optimized the energy windows which are 2–7 MeV for multi-slit system and 3–7 MeV for knife-edge system. Both energy windows include significant prompt-gamma peaks (Kozlovsky et al., 2002) such as the characteristic 4.4 MeV line due to $^{12}C(p,p^*)^{12}C^*$, $^{12}C(p,2p)^{11}B^*$ and $^{16}O(p,x)^{12}C^*$, and 6.13 MeV line from $^{16}O(p,p^*)^{16}O^*$ (Polf et al., 2009). It is reasonable that the multi-slit system requires larger energy windows to improve range detection due to its lower photon detection efficiency. In addition, there is no significant influence of the phantom size in the detection of proton range, implying that collimator-based prompt gamma cameras are suitable for various body sizes in clinical applications.

The evaluation of range shifts with simulations suggest that both collimator systems are suitable for accurately range monitoring in proton therapy when the patient is placed within a reasonable region. The accuracy of range shift prediction using knife-edge system is affected by its geometric configuration, which has a position-dependent solid angle. The distortion of profile can be significantly reduced by a shift correction process. The shift correction process needs to perform for each proton energy and knife-edge configuration employed. By contrast, the multi-slit

Table 3
Parameters estimated by a 3-line-segment curve on the detection profiles of phantom sizes of 100, 150, 200 and 300 mm with 160 MeV proton beam for both systems.

Collimator	Diameter (mm)	Peak[a]	Delta (mm)	Baseline[a]	ΔRange (mm)
Multi-slit	100	1.42 ± 0.46	8.5 ± 1.91	6.75 ± 0.26	1.28 ± 0.96
	150	1.30 ± 0.29	6.40 ± 11.78	6.71 ± 0.10	-0.47 ± 1.58
	200	1.21 ± 0.10	6.00 ± 13.56	6.52 ± 0.08	-0.27 ± 3.49
	300	1.14 ± 0.08	6.67 ± 4.62	5.32 ± 0.03	0.20 ± 2.31
Knife-edge	100	5.70 ± 0.34	34.80 ± 1.79	6.87 ± 0.26	-0.27 ± 2.86
	150	4.96 ± 0.10	35.5 ± 1.00	7.37 ± 0.01	-1.22 ± 1.50
	200	4.99 ± 0.46	35.20 ± 1.1	7.12 ± 0.13	-0.07 ± 1.52
	300	4.09 ± 0.26	34.40 ± 2.61	6.10 ± 0.16	0.33 ± 0.84

[a] The unit of the Peak and Baseline is counts $\times 10^{-7}$/proton/mm.

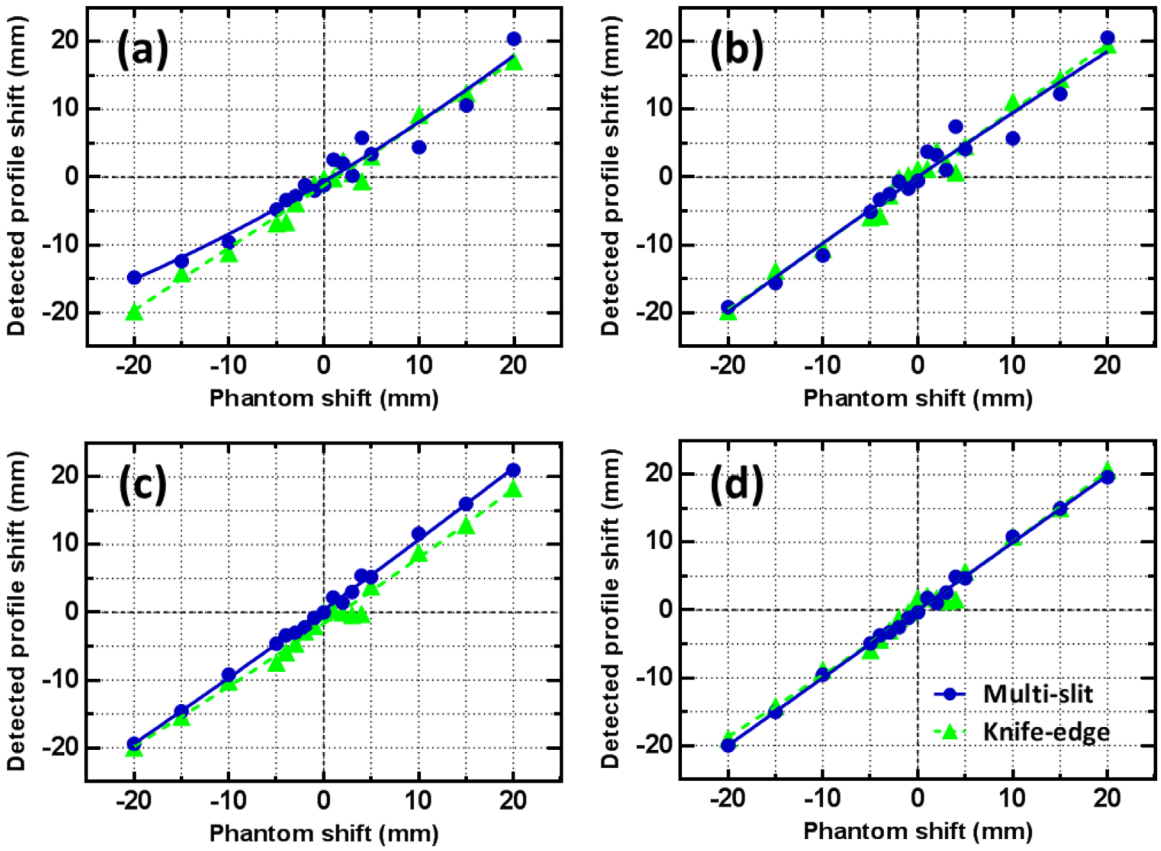

Fig. 5. The plots of detected range shift versus phantom shift in multi-slit and knife-edge systems. The top diagrams are for the detection (photon+neutron) profiles and the bottom are for photon only. The left curves are results without shift correction and the right curves are with shift correction.

system is composed of a large number of symmetrical slit collimators. This symmetrical geometric configuration makes it less affected by the phantom shift. However, the multi-slit collimator is more susceptive to the neutron contamination due to its higher neutron-to-photon ratio. A neutron rejection technique, such as a time-of-flight (TOF) technique (Biegun et al., 2012; Pinto et al., 2015) and/or a beam-tagging device (hodoscope) (Gueth et al., 2013) is important for both, especially in multi-slit system.

This study is limited only on comparing the two proposed collimator systems under the respective geometrical parameters (the collimator thickness, slit angle and slit width), even though the attempts have been made to optimize these parameters by their studies (Min et al., 2006; Smeets et al., 2012). Therefore, when comparing to multi-slit collimator, the higher detection efficiency and larger delta for knife-edge collimator can be expected due to its higher geometrical efficiency and larger slit width. The chosen of these parameters, a tradeoff between good spatial resolution and high detection efficiency, may affect these comparison results. As a result, a more equivalent comparison should be established to give a guideline of constructing a collimator-based PG camera with the desired trade-off between geometrical parameters and the limits of achievable performance. This is an area which merits further investigation.

Acknowledgments

The work was supported by Institute for Radiological Research of Chang Gung University/Chang Gung Memorial Hospital under Contract CIRPD1E0042.

References

Biegun, A.K., Seravalli, E., Lopes, P.C., Rinaldi, I., Pinto, M., Oxley, D.C., Dendooven, P., Verhaegen, F., Parodi, K., Crespo, P., 2012. Time-of-flight neutron rejection to improve prompt gamma imaging for proton range verification: a simulation study. Phys. Med. Biol. 57, 6429–6444.

Cambraia Lopes, P., Pinto, M., Simoes, H., Biegun, A., Dendooven, P., Oxley, D., Parodi, K., Schaart, D.R., Crespo, P., 2012. Optimization of collimator designs for real-time proton range verification by measuring prompt gamma rays, Nuclear Science Symposium and Medical Imaging Conference (NSS/MIC), (2012 IEEE. IEEE), pp. 3864–3870.

Grevillot, L., Bertrand, D., Dessy, F., Freud, N., Sarrut, D., 2011. A Monte Carlo pencil beam scanning model for proton treatment plan simulation using GATE/GEANT4. Phys. Med. Biol. 56, 5203–5219.

Gueth, P., Dauvergne, D., Freud, N., Létang, J., Ray, C., Testa, E., Sarrut, D., 2013. Machine learning-based patient specific prompt-gamma dose monitoring in proton therapy. Phys. Med. Biol. 58, 4563–4577.

Jan, S., Benoit, D., Becheva, E., Carlier, T., Cassol, F., Descourt, P., Frisson, T., Grevillot, L., Guigues, L., Maigne, L., 2011. GATE V6: a major enhancement of the GATE simulation platform enabling modelling of CT and radiotherapy. Phys. Med. Biol. 56, 881–901.

Kozlovsky, B., Murphy, R.J., Ramaty, R., 2002. Nuclear deexcitation gamma-ray lines from accelerated particle interactions. Astrophys. J. Suppl. Ser. 141, 523.

Lomax, A.J., Böhringer, T., Bolsi, A., Coray, D., Emert, F., Goitein, G., Jermann, M., Lin, S., Pedroni, E., Rutz, H., 2004. Treatment planning and verification of proton therapy using spot scanning: initial experiences. Med. Phys. 31, 3150–3157.

Min, C.-H., Kim, C.H., Youn, M.-Y., Kim, J.-W., 2006. Prompt gamma measurements for locating the dose falloff region in the proton therapy. Appl. Phys. Lett. 89, 183517.

Min, C.H., Lee, H.R., Kim, C.H., Lee, S.B., 2012. Development of array-type prompt gamma measurement system for in vivo range verification in proton therapy. Med. Phys. 39, 2100–2107.

Paganetti, H., 2012. Range uncertainties in proton therapy and the role of Monte Carlo simulations. Phys. Med. Biol. 57, R99.

Peterson, S., Robertson, D., Polf, J., 2010. Optimizing a three-stage Compton camera for measuring prompt gamma rays emitted during proton radiotherapy. Phys. Med. Biol. 55, 6841–6856.

Pinto, M., Bajard, M., Brons, S., Chevallier, M., Dauvergne, D., Dedes, G., De Rydt, M., Freud, N., Krimmer, J., La Tessa, C., 2015. Absolute prompt-gamma yield measurements for ion beam therapy monitoring. Phys. Med. Biol. 60, 565–594.

Polf, J., Peterson, S., Ciangaru, G., Gillin, M., Beddar, S., 2009. Prompt gamma-ray

emission from biological tissues during proton irradiation: a preliminary study. Phys. Med. Biol. 54, 731–743.
Robert, C., Dedes, G., Battistoni, G., Böhlen, T., Buvat, I., Cerutti, F., Chin, M., Ferrari, A., Gueth, P., Kurz, C., 2013. Distributions of secondary particles in proton and carbon-ion therapy: a comparison between GATE/Geant4 and FLUKA Monte Carlo codes. Phys. Med. Biol. 58, 2879–2899.
Smeets, J., Roellinghoff, F., Prieels, D., Stichelbaut, F., Benilov, A., Fiorini, C., Peloso, R., Basilavecchia, M., Frizzi, T., Dehaes, J., 2012. Prompt gamma imaging with a slit camera for real-time range control in proton therapy. Phys. Med. Biol. 57, 3371–3405.
Smith, A.R., 2009. Vision 20/20: proton therapy. Med. Phys. 36, 556–568.